CHAPTER I

INTRODUCTION/BACKGROUND

The ability of a surface to cause water to roll off or bounce away, leaving no residue behind, gives rise to the concept of superhydrophobicity.[1-5] These highly water-repellent surfaces yield extremely high contact angles when water is supported on them.[3-5] In addition, they exhibit low levels of hysteresis and wettability.[5] Close inspection of these surfaces reveals varying degrees of roughness both at the micro- and nano-scale levels, which play a role in the level of hysteresis and the degree of wettability present.[6-8] However, most methods used to prepare these types of films require the utilization of multi-step reaction sequences. More efficient methods to prepare superhydrophobic surfaces could impact a host of applications, including systems where friction reduction and slip at boundaries are important as well as stain-resistant or mildew-resistant materials and patterned surfaces used to direct the deposition of liquid precursors.[1,6]

Li et al have discussed the two primary approaches to obtain these surfaces: top-down and bottom-up.[1] In the former, utilization of templating and lithography can provide the combination of micro- and nanoscale surface roughnesses that are necessary for superhydrophobicity. This method requires several steps and can be labor intensive and costly. For example, microfabrication with photoresists must be used to achieve micro-scale roughness, whereas nanoscale roughness has been achieved by the deposition

or growth of carbon nanotubes from the micron-scale features.[2] The bottom-up approach, however, employs methods relying on self-assembly[9] and surface-initiated polymerization.[10] With this latter approach, the film is grown from the surface outward and allowed to propagate until it undergoes self-termination or the reaction is halted.[11] Here, the surface roughness necessary for the appearance of superhydrophobic properties may arise naturally from the randomness with which the growing polymer chains terminate, making this approach less labor intensive as no templating or patterning steps are required.

Gao and McCarthy reported obtaining "perfectly hydrophobic" (i.e. contact angle = 180°) surfaces 70% of the time when growing a methylsilicone network from a silicon wafer.[3] The fact that these "perfect" surfaces were not produced in a completely reproducible manner was related to fluctuations in background humidity levels. While this is probably an ideal case, preparation of these types of films can take place in many ways to provide superhydrophobic films. One example of the application of the bottom-up approach involves the application of surface-initiated polymerization to grow PS from a film of oriented carbon nanotubes. In 2006, Li et al.[1] reported the construction of artifical lotus leaf (the biological plant known for its water repellancy) structures on cotton textiles using carbon nanotubes. This was typically done using chemical vapor deposition (CVD) onto the carbon nanotube surface and depending on spacing between nanotubes, the surface was either hydrophobic or hydrophilic. Sun[2] was successful in an attempt to achieve superhydrophobic monolayers on a GaAs surface by first utilizing a layer of Ag nanoplates. When large rough Ag nanoplates were deposited onto the GaAs

surface, these resulting substrate exhibited the "Lotus" effect and obeyed the Cassie nonwetting state.[2]

While the various approaches to generate superhydrophobic surfaces described above have proven to be successful, a more advantageous approach would be the development of a single-step polymerization method that could produce films with superhydrophobic behavior. Here, we introduce a new approach for the growth of superhydrophobic films from a single-step polymerization. In this approach, diazomethane is exposed to a borane-terminated self-assembled monolayer (SAM) to insert methylene $-(CH_2)-$ species between the B-C bond and extend a growing polymethylene (PM) chain from the surface. This strategy is essentially a surface-initiated form of polymerization that has been pioneered by the Shea group.[12-14] Growth from the surface continues spontaneously as long as the concentration of diazomethane in solution is sufficient or until the chains terminate. The complex interplay of chain density on the surface and the reaction rate for chain termination affects the morphology of the film surface and in certain extremes, can promote superhydrophobic behavior. Given that the chains could terminate at different times and lengths, the surface roughness necessary from superhydrophobicity can arise. Aside from the condensation-based polymerization of silane precursors, surface-initiated polymer films from 2-D substrates that yield superhydrophobic surfaces have not been reported to date.

Polyhomologation

Shea and co-workers have introduced a synthetically elegant method known as polyhomologation for generating end-functionalized polymethylene ($R(CH_2)_nX$; where X

commonly is –OH and R is one of various terminal groups) by reacting dimethylsulfoxonium methylide ($CH_2S(O)Me_2$) with an alkyl borane, as shown in Scheme I:[12]

Scheme I

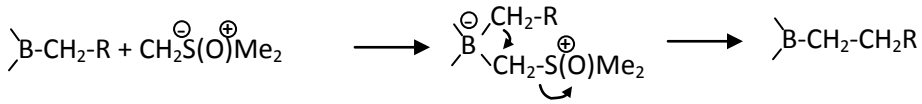

The product of this 1,2 migration of the alkyl group can react with additional ylide to extend the chain length. Because the chain can propagate from each of the three arms of the borane (not shown in the scheme), the chain lengths are statistically similar, keeping polydispersities low. Quenching of the reaction with basic peroxide produces an alcohol-terminated polymethylene that can be chemically converted to various functional groups (X).[12] In addition, the R-group terminating the opposite end of the chain can be selected by reacting an R-terminated olefin with diborane (B_2H_6) prior to introducing the ylide in Scheme I.[13] Shea and co-workers have demonstrated that various R groups, including alkyl-,[12] $MeO(CH_2CH_2O)_n(CH_2)_3$-,[13] and MeO(phenyl)$(CH_2)_2$-,[14] are compatible with this synthetic procedure. The primary advantages of using polyhomologation to synthesize end-functionalized polymers include low polydispersities (1.01-1.17) and tight control over chain molecular weight by varying the ratio of ylide to trialkylborane. In this thesis, I have extended the Shea approach to produce surface-initiated polymethylene films that are grown from borane-terminated self-assembled monolayers (SAMs).

Surface-Catalyzed Growth of Polymethylene

Allara and co-workers[15] reported an extremely convenient strategy for forming ultrathin polymethylene [-$(CH_2)_n$-; PM] films and clusters on gold surfaces by simply immersing

the substrate in an ethereal solution containing diazomethane (CH_2N_2; DM). DM decomposes at the catalytic gold surface to produce an adsorbed methylidene species that initiates a polymerization:

$$n\ CH_2N_2 \prod \text{-}(CH_2)_n\text{-(surface)} + n\ N_2\ (g) \qquad (1)$$

The polymerization results in isolated clusters of PM on the gold surface at short times; these clusters eventually coalesce to yield a film with an asymptotic thickness of up to 100 nm. As the PM films form by initiation at a surface, they can be applied to various geometries—including the internal walls of small tubes and in tiny crevices—that are difficult, if not impossible, to coat by other methods of application. The convenient processing of these PM films, combined with the superior barrier properties and chemical stability of polyolefins, yields a potentially simple and effective strategy for forming ultrathin films that function as resistors or barrier films.[16] This straightforward processing strategy is particularly useful since many polyolefins suffer from poor processibility and cannot be solution-cast or spin-coated.[15] Drawbacks to this approach include the limitations on film thickness (up to ~100 nm) and substrate (limited to gold).

Guo and Jennings[17] later showed that the surface-catalyzed growth of PM is greatly enhanced if a submonolayer of copper is deposited on the gold surface but is prevented if a monolayer of silver is instead deposited prior to polymerization. They used this approach to direct the growth of PM films on a pre-patterned substrate.[18] The use of a silver monolayer to inhibit PM growth from gold is used throughout this work to enable separation of the effects of the surface-initiated polyhomologation from the surface-catalyzed polymerization.

Here, I introduce the use of a surface-initiated polyhomologation approach to grow films from Au surfaces, but using diazomethane as the methylene source. Early on in this project, other researchers in the Jennings group noted that many of the PM surfaces grown by this approach exhibited very large advancing and receding contact angles and could be classified as superhydrophobic. This thesis focuses on the processing conditions that promote the generation of superhydrophobic surfaces and also investigates the stability of the superhydrophobic condition to long-term water and heat exposure. As extentions of this work, I additionally propose methods for patterning the superhydrophobicity of these interfaces.

Polymethylene films were prepared on gold surfaces with and without an atomic layer of silver. In both cases, the vinyl thiol and subsequent borane groups were attached, and polymerization was allowed to occur via introduction of a 8.5 mM solution of diazomethane in ether at -17°C. For the case of Au, polymerization is initiated not only at the borane sites, but can also take place at the Au surface as well to generate two distinct types of PM chains.[15] In an effort to determine if this surface-catalyzed polymerization has an effect on the overall superhydrophobic nature of these films, the Ag/Au substrates were utilized. The Ag layer was deposited by upd and is known to contain a coverage of 0.9-1.0, which has been shown by Guo and Jennings to prevent the direct surface-catalyzed polymerization to form PM.[18] In this case, polymerization is limited to the borane sites, thus leaving the presence of surface-catalyzed polymer growth as the only difference between the two films. Figure 1.1 depicts the reaction scheme utilized in the preparation of PM films on the Ag/Au substrate. A schematic for the Au

substrate would be similar except there would be PM chains propagating from the Au surface in the final step in addition to the borane sites shown here.

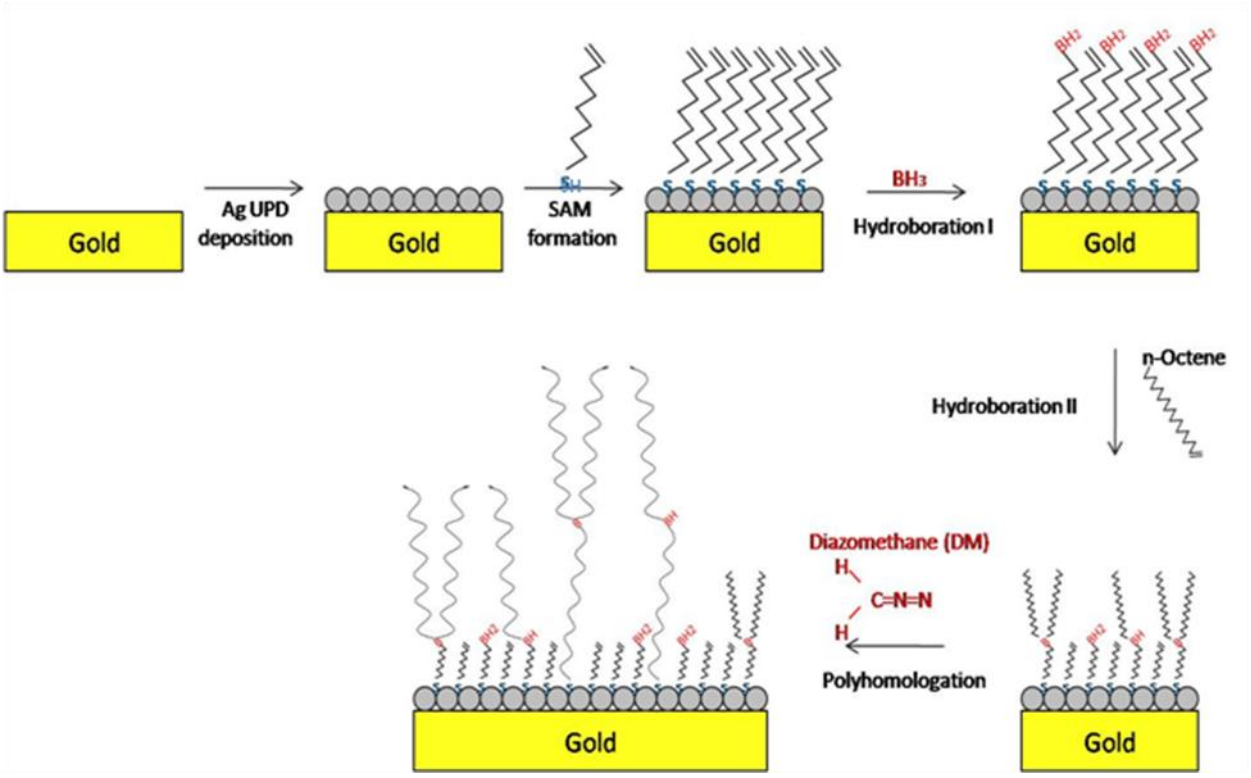

Figure 1.1. Schematic of reaction steps for growing PM films from a Ag/Au surface. These films can also be grown from Au (no Ag) by the same process and from silicon if the surface is modified by a vinyl-terminated trichlorosilane prior to hydroboration.

Characterization of these films included several methods for identifying not only their overall performance, but also, how the films compare to one another. During the polymerization, the infrared absorbance was monitored at set time scales to identify how this polymerization proceeds over time. RAIR spectroscopy was utilized predominately to track the progression of the PM film growth because ellipsometric techniques that employed a Cauchy model gave large errors and did not yield accurate values of thickness for the thicker films in this study (a few microns in thickness). I did compare

the IR absorbance with average thicknesses obtained from QCM measurements. I also examined the structual morphology with AFM and SEM to probe surface roughness with continued polymerization and to identify any differences between films grown from the different substrates. In addition, some insight on the overall packing/crystallinity of these films was examined using RAIR spectroscopy by quantifying relative peak ratios for C-H rocking modes at 719 and 730 cm^{-1} as described by Allara.[15] Lastly, the stability of the superhydrophobicity exhibited by these films with respect to water, heat, and solvent (trichlorobenzene) exposure was investigated in attempts to identify potential applications.

CHAPTER II

EXPERIMENTAL

Materials

Ethanol (ACS/USP grade) was used as received from AAPER. Thiolacetic acid (98%) was obtained from Acros Organics. Sodium hydroxide (ACS grade), potassium hydroxide (ACS grade), hexane (HPLC grade), hydrochloric acid (36.5-38%), and concentrated sulfuric acid (95-98%) were used as received from EMD Chemicals. Sodium methoxide (>97%) and nitrogen gas were obtained from Fluka and J&M Cylinder Gas, Inc, respectively. 11-Bromo-1-undecene (95%), 1-octene (98%), borane-tetrahydrofuran (THF) complex solution (1.0 M), diazald (*N*-methyl-*N*-nitroso-*P*-toluenesulfonamide, 99%), diethyl ether anhydrous (>99%), phenolphthalein (ACS grade), silver sulfate (99.999%), and tetrahydrofuran anhydrous (>99.9%) were acquired from Sigma-Aldrich. Deionized water (16.7 MΩ•cm) was purified using a Modu-Pure system and used for electrochemical characterizations and rinsing. Gold shot (99.99%) and chromium-coated tungsten filaments were purchased from J&J Materials and R. D. Mathis, respectively. Silicon wafers (100) were obtained from Montco Silicon, rinsed with water and ethanol, and dried in a stream of nitrogen.

Synthesis of Undec-10-ene-1-thiol

The thiol was synthesized from the corresponding bromide by using acidic solvolysis conditions. Under a nitrogen atomosphere 11-bromo-1-undecene (1.543 g) and thiolacetic acid (0.529 g) were added to 61 mL of methanol in a stirred flask. The system reacted for 10 h under reflux and thin film chromatography (TLC) with hexane as solvent was used to determine the end of the reaction. After the bromide completely reacted, hydrochloric acid was added to the system under inert atmosphere and reacted for 12 h. Depletion of the acetate was determined by TLC using a solution of hexane/ethyl acetate (30/1) as solvent. At the end of the reaction, the product was dissolved in hexane, washed with water, and dried with calcium chloride. To purify the thiol, the organic phase was concentrated using rotary evaporation and then separated using column chromatography with a solution of hexane/ethyl acetate (30/1). Finally, the thiol was concentrated using vacuum distillation.

Preparation of Diazomethane

Utilizing a mini-diazald apparatus purchased from Sigma-Aldrich, a mixture of ethanol/KOH/water (10 mL/5 g/8 mL respectively) at 65°C was charged with a solution of diazald in ether to produce diazomethane gas. The DM gas was condensed with ether via a dry ice/acetone condenser. The resulting distillate was then diluted with additional ethyl ether to produce a concentration of 8.5 mM DM. For a more detailed procedure consult Aldrichimica Acta.[19]

Film Preparation

In order to synthesize the substrates necessary for the experiments, Au and Ag-plated Au (denoted as Ag/Au) substrates were prepared. Layers of chromium (10 nm) and Au (~ 150 nm) were evaporated in sequence onto a silicon wafer at a base pressure of 4×10^{-6} Torr. This wafer was cut into 1 cm x 4 cm sections to yield the Au substrates needed for polymerization. All substrates were then washed with copious amounts of water and absolute ethanol. After the final ethanol rinse, each substrate was dried using a stream of nitrogen. The substrates were used as the working electrodes in electrochemical cells to plate approximate monolayers of Ag through underpotential deposition (UPD) from a 0.1 M H_2SO_4 solution containing 0.6 mM $AgSO_4$ (counter electrode = gold-coated silicon). On the cathodic scan, the potential was held at 60 mV vs $Ag^{+/0}$ reference, and the working electrode was removed from the cell under potential control and immediately rinsed with ethanol and dried in a stream of nitrogen. Each of these films (in groups of four) were submersed in a 1 mM ethanol solution containing undec-10-ene-1-thio1 for 24 h to achieve a dense vinyl-terminated SAM. After removal from solution, the SAM-coated films were rinsed with ethanol and water and dried in a stream of nitrogen.

Au and/or Ag/Au substrates that were modified by the vinyl-terminated SAM were sealed in a vial under nitrogen by evacuating the vial and then refilling with nitrogen, and repeating two more times. Then, 2 mL of 1 M borane in tetrahydrofuran (THF) was diluted to 20 mL with anhydrous THF and added via canula and allowed to react under nitrogen for 2 h. After reaction, the system was rinsed three times with anhydrous THF via canula under nitrogen to remove all traces of remaining borane.

Next, 258 µL of 1 M octene in THF was purged with nitrogen and diluted to 20 mL with THF to create a 13 mM solution. The octene:THF solution was added to the vial holding the samples via canula and an additional 2 h was allowed for the octene to react with the surface-bound borane molecules. The reaction vessel was again rinsed three times with anyhydrous THF.

Samples were removed from the reaction vessel through air and placed into a chilled vial of 8.5 mM diazomethane in ethyl ether at -17°C to grow the polymer film. The reaction began immediately as indicated by rapid bubbling that slowed over time. The reaction vessels were placed in a freezer at -17°C for the duration of the polymerization. This step alone is the single-step polymerization that will ultimately yield superhydrophobic polymethylene films.

Electrochemical Impedance Spectroscopy

Electrochemical impedance spectroscopy (EIS) is an analytical technique that can be very useful in examining the barrier properties of an organic thin film, in particular, the resistance of these films against the transport of ions from solution and the capacitance of the films when in contact with an electrolyte solution.[17-18] During this process, the potential applied to the circuit element is varied in a sinusoidal fashion while the current is measured. This current measurement allows calculation of the impedance via the following relation:

$$Z = E / I \qquad (1)$$

where Z is the impedance calculated using the current (I) and potential (E). The resistive and capacitive values for the film can be determined by fitting impedance data with an appropriate model, such as a Randles equivalent circuit model (Figure 2.1).[20,21]

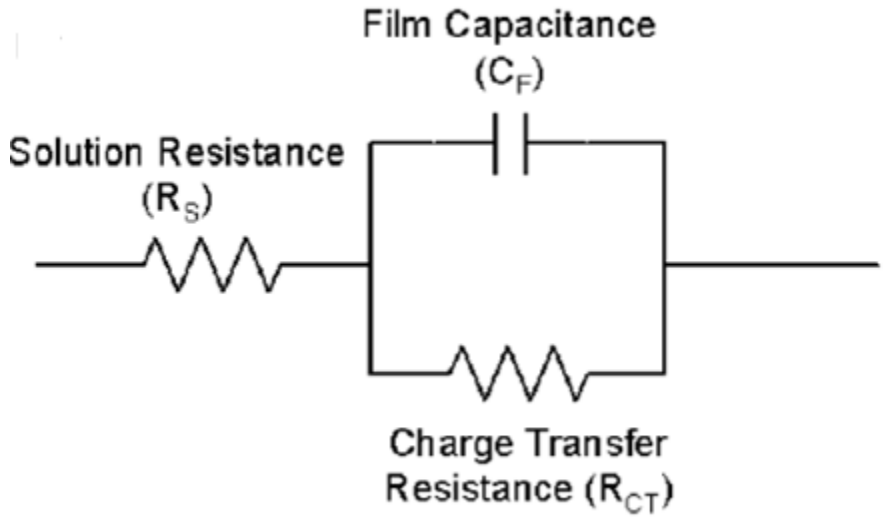

Figure 2.1. Illustration of a Randles circuit used to model electrochemical impedance data.

The Randles circuit contains a solution resistance in series with a parallel combination of film capacitance and film resistance. Depending on the frequency, any one of these circuit elements could provide the dominant impedance. For example, at high frequencies, the resistance of the electrolyte solution (Ωs) is often detected because the sinusoidal potential changes too rapidly to probe film properties. At intermediate frequencies, the film often behaves as a capacitor, separating the ions from the conductive metal substrate, as ions are unable to diffuse into the film due to insufficient time to penetrate the film before the sinusoidal potential changes. At low frequencies, sufficient time exists for the ions to penetrate the film, and the film provides a resistance

against the ions as they diffuse towards the electrode surface. Log-log plots of the impedance modulus versus frequency are called Bode plots[20] and can be used to graphically represent the transformations in impedance with changing frequency. In the Bode plot shown in Figure 2.2, the solution resistance is shown at highest frequencies as a leveling of the spectrum, the capacitance from 20 to 1000 Hz as a linear segment with a slope approaching -1, and the film resistance at low frequencies as another flat portion of the spectrum.

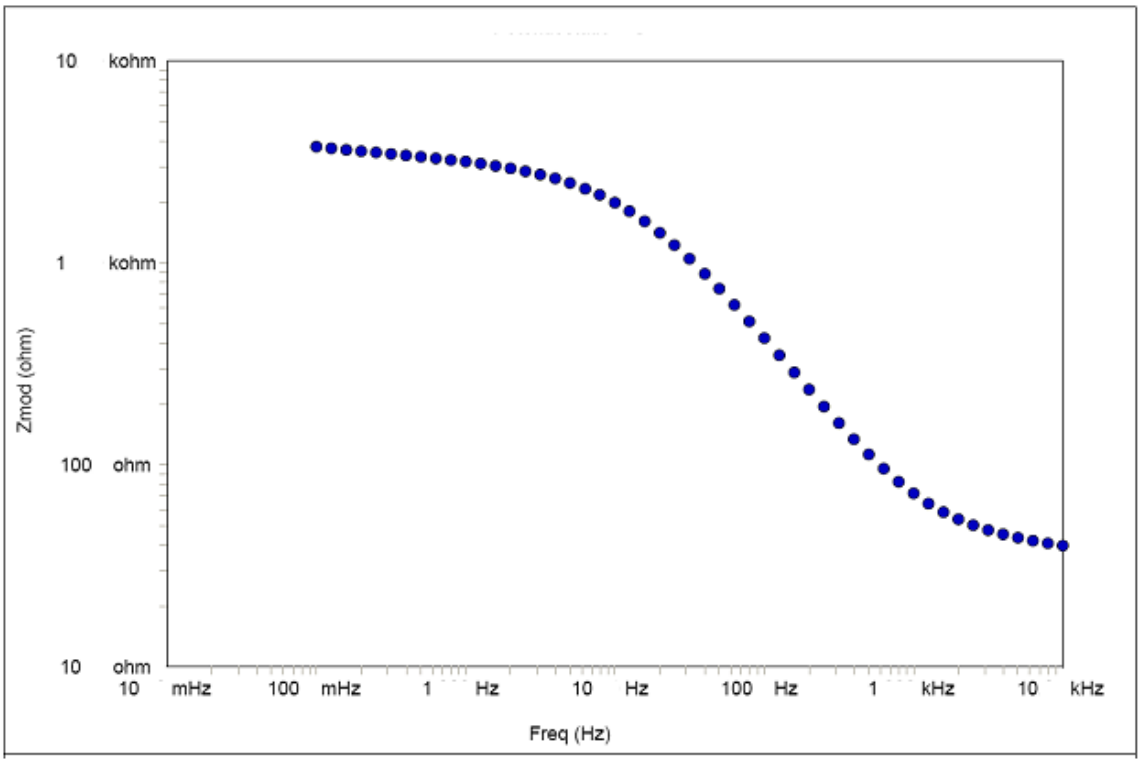

Figure 2.2. Bode plot resulting from the electrochemical impedance of a PM film grown on a Au surface as tested in 0.1 M Na_2SO_4(aq) containing 1 mM $K_3Fe(CN)_6$ and 1 mM $K_4Fe(CN)_6$ as redox probes.

Infrared Spectroscopy

Reflectance absorption infrared spectroscopy (RAIRS) can be a useful tool in the investigation of the composition and structure of an organic thin film. An infrared beam of light is reflected off the film surface and passed onto a detector. The difference in intensity between the beam reflected off a pure Au surface and a PM-coated Au surface quantifies how much light is absorbed by the PM itself. In this application, infrared radiation over a wide range of frequencies is absorbed by molecular groups within the film and is quantized as being the difference in intensity that is produced by the source and collected by the detector. Depending on the composition of the film, certain wavelengths of radiation are absorbed while others are completely reflected. For polymethylene films there are three frequencies that can provide useful information:[15] the 2800-3000 cm^{-1} region where C-H bonds exhibit stretching vibrations, the 1460-1480 cm^{-1} region, where these same C-H bonds exhibit bending vibrations, and from 719-730 cm^{-1}, where C-H bonds exhibit rocking vibrations. Various structural characteristics such as the degree of symmetric vs. asymmetric vibration can be determined at specific wavenumbers and related to film structure.[22] In addition, peak splitting and their relative ratios can provide information on the overall order and crystalline packing of the structure.[15] Studies have shown a splitting for the rocking band of polymethylene at 720 and 730 cm^{-1} and have determined that the intensity ratio (I_{720}/I_{730}) of 1.233 for pure orthorhombic crystalline packing.[22] In addition, amorphous phases can give rise to single peaks in this region that might skew the determination of crystallinity.[15] Such a peak may occur around 718 cm^{-1} and interfere with the determination of orthorhombic character as only orthorhombic packing can cause the observed splitting with the 720 and 730 cm^{-1}

peaks. In addition, levels of absorbance can provide some correlation to the thickness of these films as thicker films would generally contain more CH_2 groups and thus higher absorbance values.

Contact Angle Measurements

The measurement of contact angles can be utilized to determine how certain liquids interact with the surface of an organic thin film and provide insight on the interfacial free energy and composition of surfaces. The process involves placing a drop of liquid (usually water) on the surface of the film and measuring its contact angle with a goniometer. The angle (θ) is a function of the surface tension of the liquid (γ_{LV}) as well as the free energies of both the solid-air (γ_S) and solid-liquid (γ_{SL}) interfaces, according to Young's equation:[23]

$$\gamma_{SL} + \gamma_{LV} \cos\theta = \gamma_S \qquad (2)$$

In general there are two types of contact angles: advancing and receding. An advancing contact angle is that is measured after a liquid has been advanced across a surface while a receding contact angle is obtained after some of the liquid has been removed from the surface. The difference between these two values is called the hysteresis.

Of particular interest are films that can be classified as superhydrophobic, in which the water contact angles (both advancing and receding) are above 150-160°. Zhu et al.[24] reported contact angles as high as 168° for work done on carbon nanotube arrays. In addition they obtained hysteresis values of less than 1° indicating the high level of superhydrophobicity of their films.[24]

Atomic Force Microscopy

In this method of substrate analysis, a micron-sized cantilever is scanned over the film surface in order to investigate its topology. As the cantilever is brought into the presence of the surface deflection occurs and is measured by an array of photodiodes. AFM can be used to image almost any type of surface such as polymers, composites, and glass. The specific mode of AFM used here is tapping-mode, in which the cantilever is oscillating at a preset frequency of cycles per second.[15] Contact with the surface alters the oscillation and gives rise to an energy loss. Thus, the surface features can be identified and measured by this reduction in oscillation. It should be noted however that this can also occur without surface contact as well.

Scanning Electron Microscopy

Scanning electron microscopes utilize a high-energy beam of electrons to interact with the atoms on a surface. The beam is focused on the surface by a series of magnetic lenses. The electrons hitting the surface cause secondary electrons to be emitted from the surface, their energy being dependent on the element from which they originate. These electrons are counted by the detector and corresponding signals are sent to the amplifier. The resulting image is defined by the quantity of electrons of different energies emitted from each location during the scanning process.

CHAPTER III

RESULTS AND DISCUSSION

Figure 3.1 displays a typical IR spectrum obtained for the PM films and illustrates the key features indicative of PM. The PM film in this case arises from surface-initiated polymerization from borane-modifed Au that has been exposed to DM for 1 h at -17°C. Vibrational modes due to C-H stretching, C-H bending, and C-H rocking are present at 2850-2920, 1463-1473, and 719-730 cm^{-1}, respectively. The absence of absorbance peaks due to CH_3 stretching indicates that the polymer is predominately, if not completely, linear polymethylene, as expected from a polyhomologation-type reaction. For the purpose of these studies, I focused on the C-H bending and rocking signals due to their consistent form throughout the polymerization. Signals for the stretching mode were so strong even at these low thicknesses that the signals saturated the detector proventing accurate quantification. For example, the thicker films yielded some negative absorbance in the C-H stretching region at long times, but the bending and rocking signals show steady increases with time.[25]

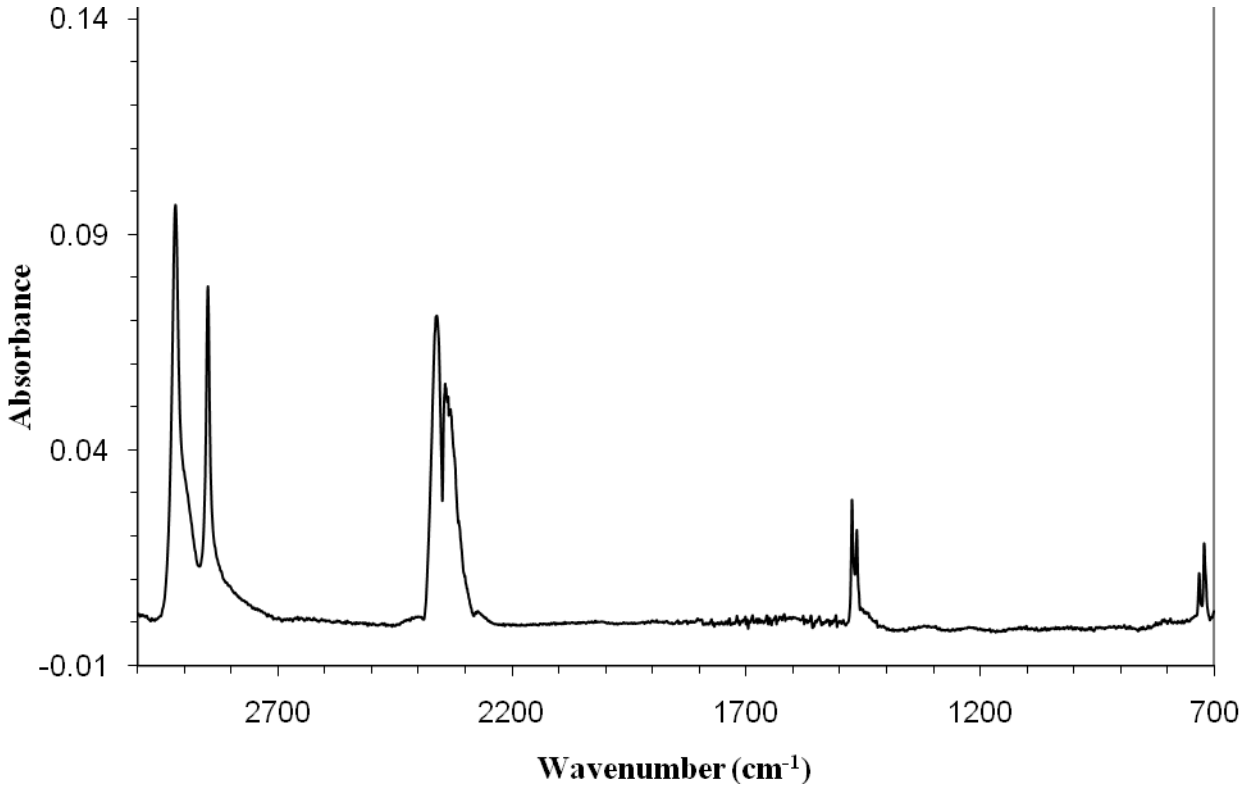

Figure 3.1. RAIR spectrum obtained for PM film grown from borane-modified Au surface after exposure to 8.5 mM DM in ether at -17°C for 1 h.

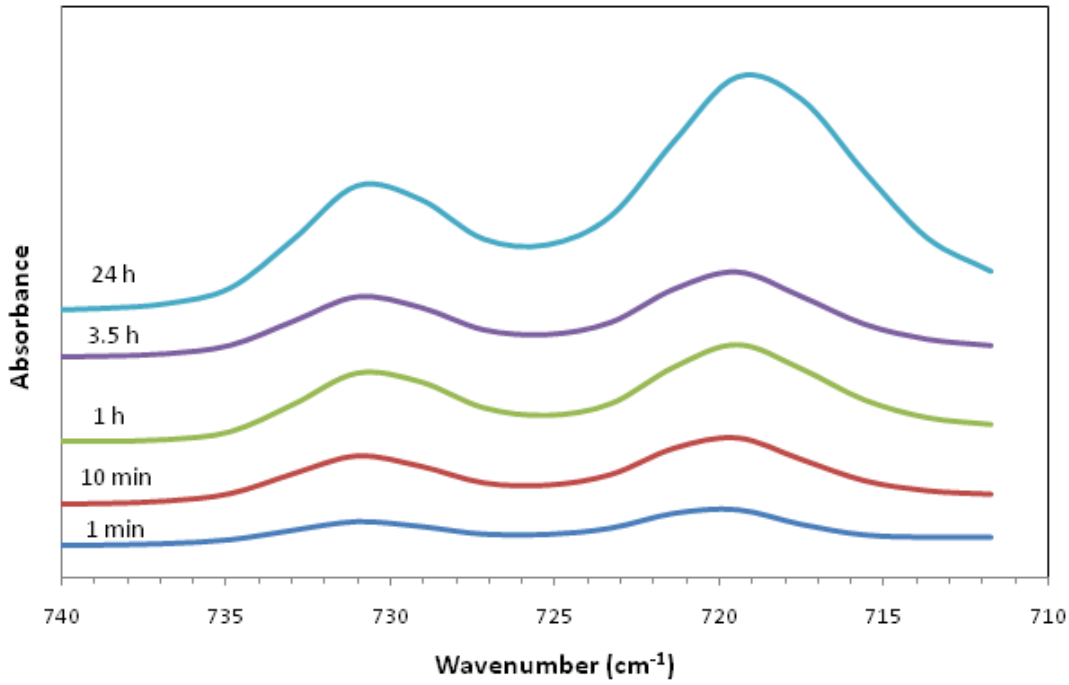

Figure 3.2. Infrared absorbance for C-H rocking signals of PM films grown on borane-modified Au surfaces that were exposed to 8.5 mM DM in ether at -17 °C for 1 min to 24 h.

Figure 3.2 shows IR spectra of the C-H rocking modes to illustrate the changes in the overall structure of these PM films as they grow. The rocking modes occur from 719-730 cm^{-1} and are split peaks for C-H bonds of PM due to the vibrations in and out of plane with respect to the rest of the molecule.[15] The absorbance ratio of the 730 to 719 peaks would suggest orthorhombic crystalline packing if they were equal to 1.233. At short times, the ratios are ~1, suggesting more orthorhombic-like packing in the PM films on both Au and Ag/Au. However, observation of the ratio of these two peaks after longer polymerization times, in particular 24 h, shows that as the films become thicker, this ratio trends toward ~0.33 suggesting that other types of chain packing, such as mono-clinic,

occur in the film as it becomes thicker. Some IR spectra show a shoulder peak at 718 cm^{-1}, which according to Allara, is indicative of monoclinic packing as the film grows.[15]

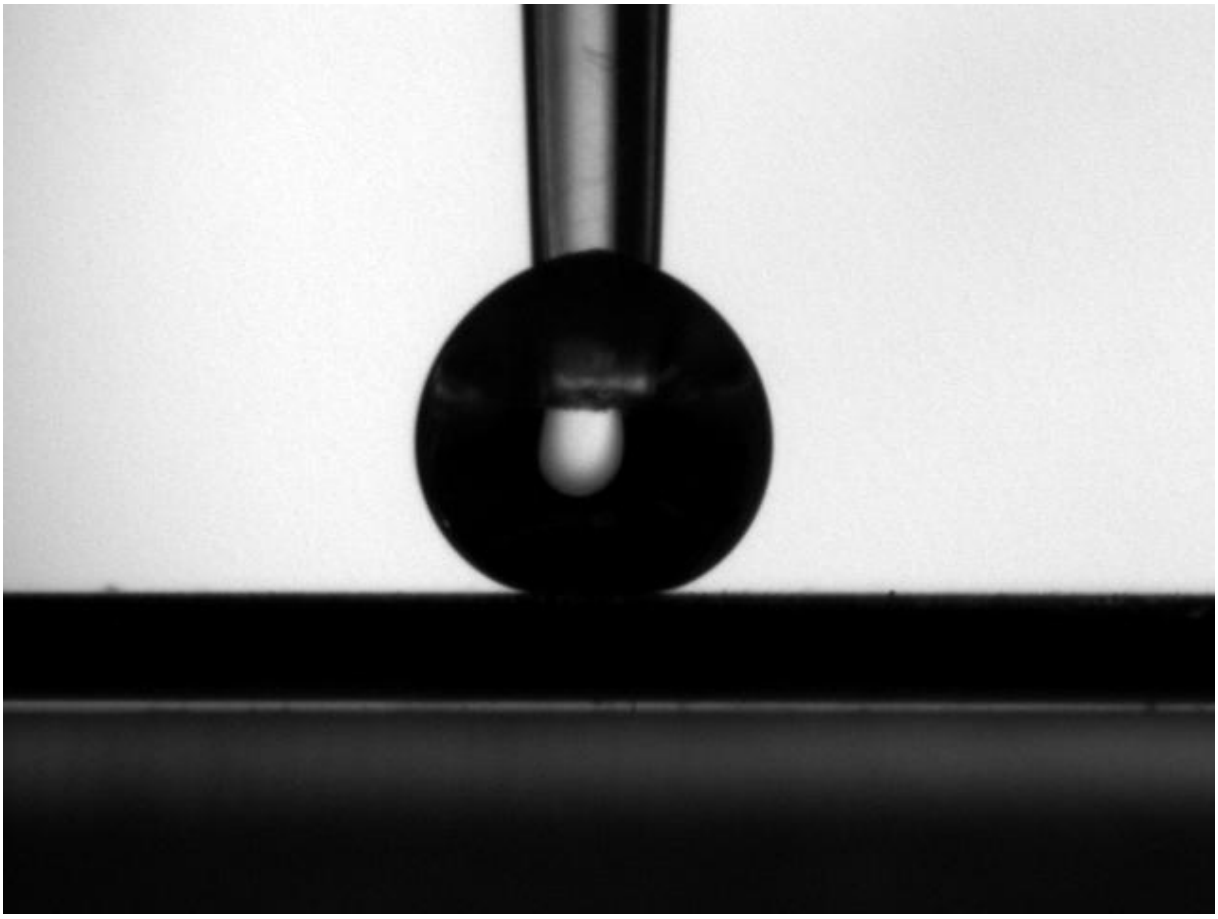

Figure 3.3. Picture of a water droplet on a PM surface that exhibits an advancing contact angle of ~160°.

To characterize the surface properties of PM films grown from both Au and Ag/Au surfaces, contact angles of water were measured. The extreme superhydrophobic nature of the film gives rise to droplets whose area of surface contact is minimal, resulting in advancing contact angles of ~150-160° for PM on Au and Ag/Au. In

addition, receding contact angles were also ~150-160°. The low level of hysteresis was indicative of the superhydrophobicity of these films.

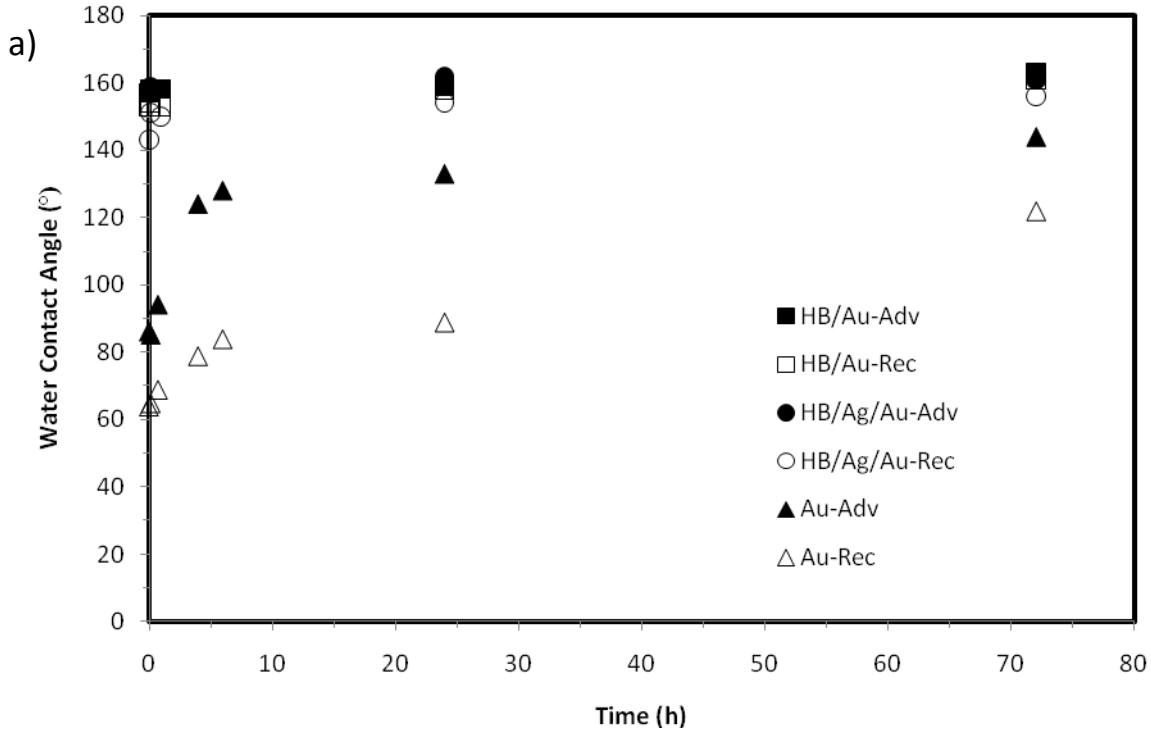

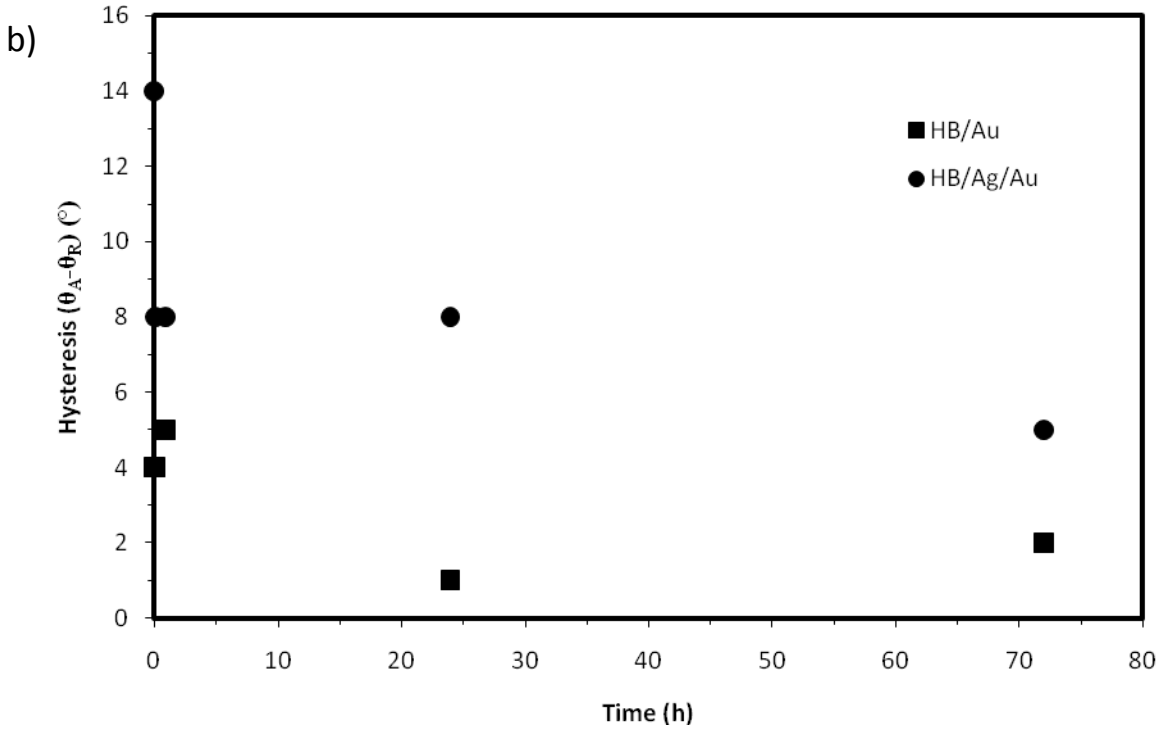

Figure 3.4. Advancing and receding water contact angles (a) and hystereses (b) for PM grown on borane-modified (HB = hydroborated) Au and Ag/Au surfaces and unfunctionalized Au after exposure to 8.5 mM DM in ether at -17 °C for the times indicated.

To examine the effect that the PM film has on wettability, Figure 3.4a shows the advancing and receding contact angles for H_2O on Au and Ag/Au surfaces after exposure to 8.5 mM DM in ether at -17 °C for up to 72 h. If superhydrophobicity is defined as both advancing and receding contact angles that are > 150°, PM films grown from both Au and Ag/Au surfaces exhibit superhydrophobic properties after the first 1 and 10 min of growth, respectively, indicating that even at these early times of polymerization, there is sufficient PM growth to elicit a superhydrophobic response. In contrast, PM films grown directly from Au (no HB) do not exhibit superhydrophobic properties even after

72 h of growth. These surface-catalyzed PM films are much thinner than the PM films grown by HB surfaces and are known to be relatively smooth.[18] The hysteresis for PM films grown from HB surfaces decreases with time and is slightly larger for PM on HB/Ag/Au than for PM on HB/Au. A low hysteresis has been correlated with the ability of contacting droplets to roll off the surface with minimal tilting of the substrate.[5] The low hysteresis for PM grown from HB surfaces in contrast to that grown directly from Au suggests a morphological effect on wettability.

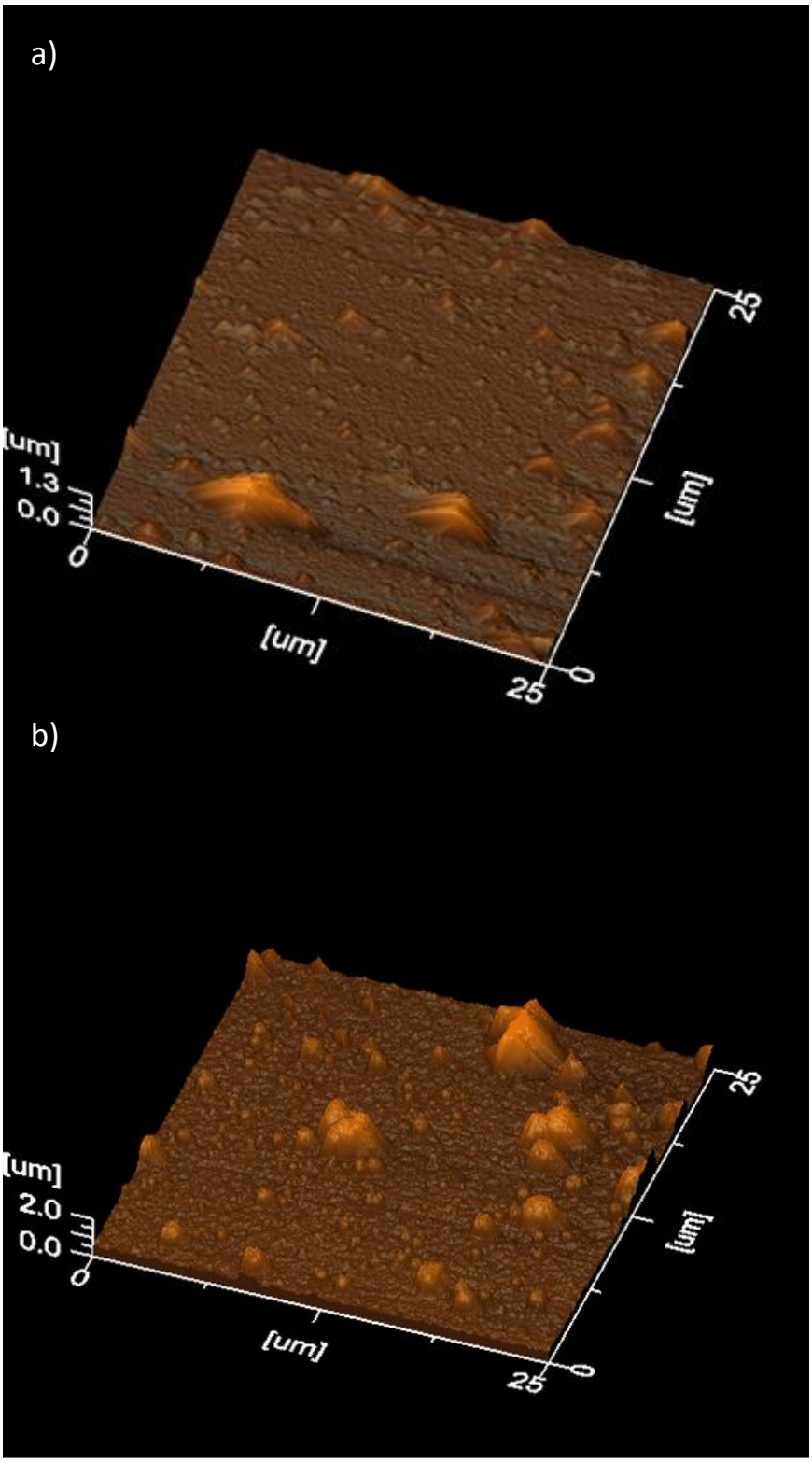
a)
[um]
1.3
0.0
0
[um]
25
0
25
[um]
b)
[um]
2.0
0.0
0
[um]
25
0
25
[um]

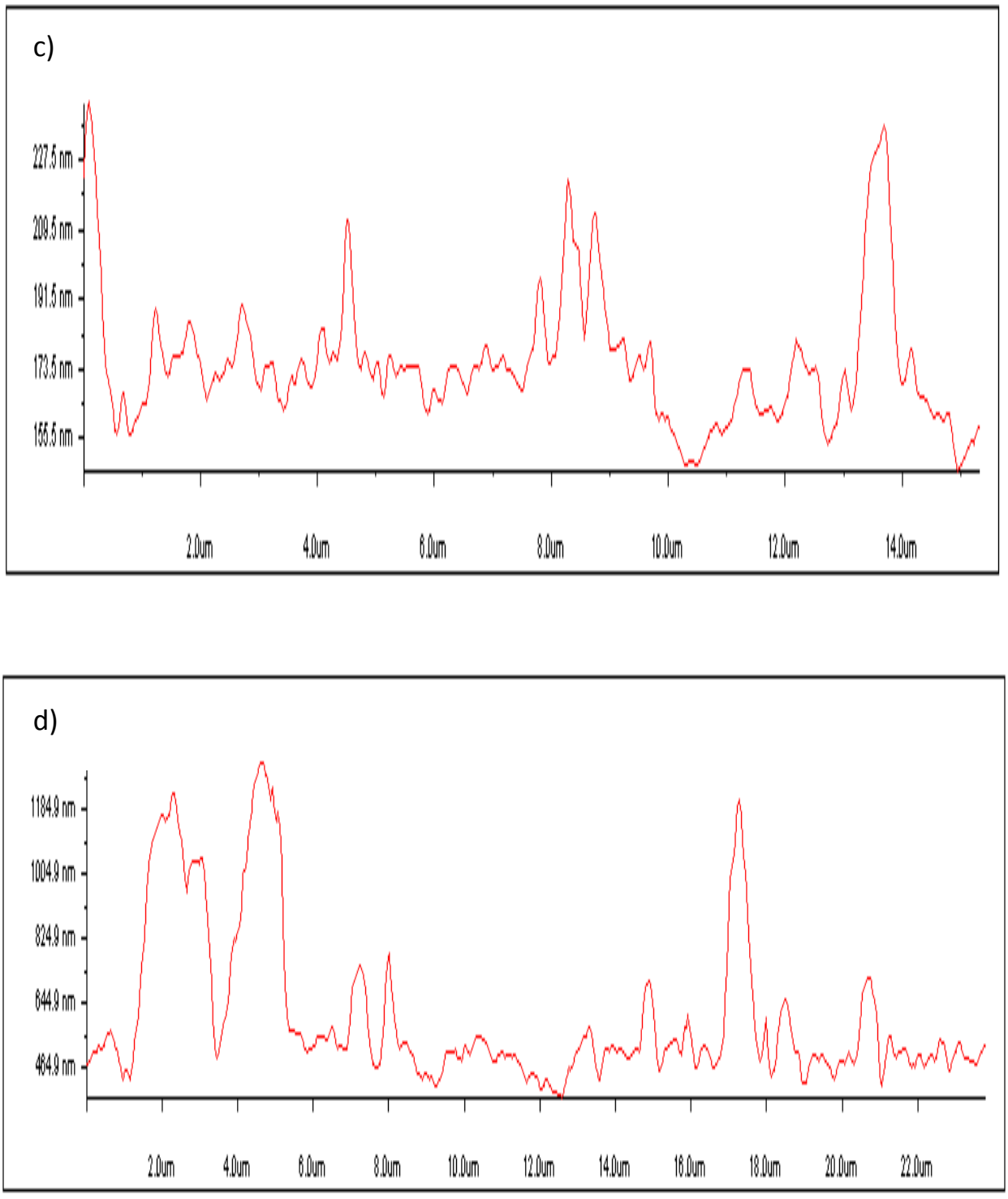

Figure 3.5. AFM images (a and b) and line scans (c and d) of PM films grown from borane-modified Ag/Au surfaces from 8.5 mM DM in ether at -17 °C for 10 min (a and c) and 24 h (b and d). The morphologies for films grown from HB/Au (not shown) are similar.

Figures 3.5 shows AFM images and lines scans for PM films grown from borane-terminated Ag/Au surfaces after 10 min and 24 h, respectively, and were obtained to illustrate the change in the overall surface features of the film as it grows with time. The first image was obtained after 10 min of growth where the surface contains many small features that are (~500 nm in diameter and 250 nm high according to the line scan in Figure 3.5c) and a few large features (~5 μm in diameter and ~1 μm high). The combination of micron- and nanometer-scale roughness likely explains the very large water contact angles on this surface, even at these early stages of polymerization. Allowing the film to grow 24 h results in the topology shown in Figure 3.5b and d. Here, the film is noticeably rougher with a large degree of small peaks scattered throughout, and a few larger surface features on the order of 2.0 μm in height, twice as tall as those shown in Figure 3.5a. In general, the 24 h film demonstrate the same key features of the 10 min film, but these features have continued to grow and, in the case of the smaller peaks, multiply. This result suggests that initiation does not occur simultaneously across the surface and that all sites are not equal. While all the chains will eventually terminate, the gradual termination of chains across the surface with time, combined with different chain densities and propagation rates, gives rise to the varied structural morphologies across the surfaces. The sheer difference in the amount of peaks seen in the two images gives some insight to the degree of roughness present in the two films but only reflects a small difference in superhydrophobicity based solely on advancing contact angle measurements and a substantial difference in hysteresis. While the advancing contact angles are high for both films, the receding angle climbs 5 to 10° over this time period to increase the superhydrophobicity. Correlation of these images with contact angle

measurements suggests that more pronounced micro- and nanoscale roughnesses lead to lower contact angle hystereses for superhydrophobic polymer films.

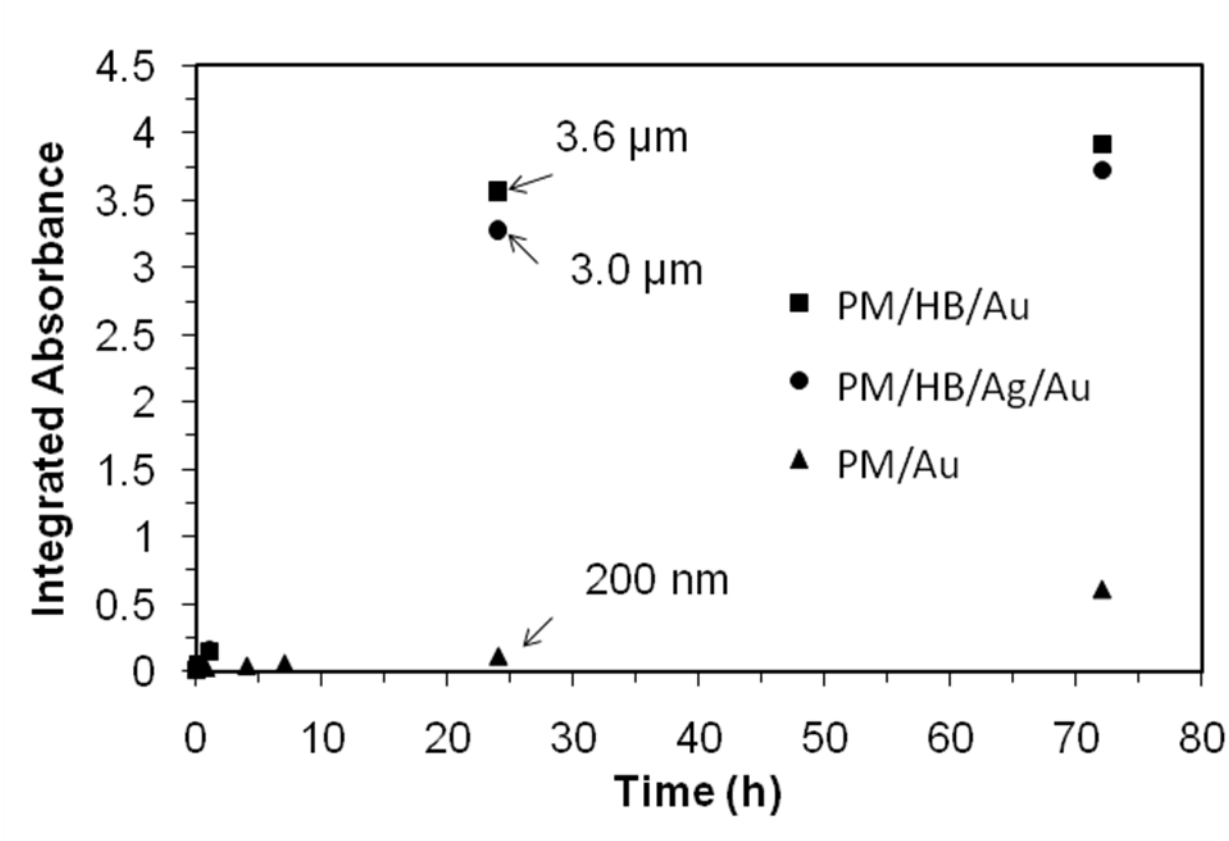

Figure 3.6. Integrated absorbance of the C-H bending peaks at 1463 and 1473 cm^{-1} from infrared spectroscopy for PM films grown from borane-modified Au and Ag/Au surfaces and unfunctionalized Au after exposure to 8.5 mM DM in ether at -17°C for the times indicated. The average thickness of the 24-h films by QCM are 3.6 µm, 3.0 µm, and 0.2 µm for PM grown from HB/Au, HB/Ag/Au, and Au, respectively.

Figure 3.6 shows the relation between polymerization time and integrated absorbance for C-H bending of PM films on hydroborated Au and Ag/Au surfaces, as well as unmodified Au. The absorbance depends on the number of CH_2 groups in the PM film, which scales with the thickness of the film, and the orientation of their transition

dipole moments with respect to the surface normal. The overall trend in C-H bending absorbance is similar for PM growth from hydroborated Au and Ag/Au surfaces at times ranging from 1-72 h with slight differences that may reflect the role of surface-catalyzed polymerization from gold to slightly enhance the overall thickness of that film. The PM film grown from a non-hydroborated surface shows a relatively weak absorbance, consistent, with a much slower polymerization. At 24 h of growth, the thicknesses of the films from QCM are 3.6 μm, 3.0 μm, and 0.2 μm for PM grown from hydroborated Au and Ag/Au as well as unmodified Au, respectively. Therefore, the presence of the borane greatly increases the overall rate of PM growth and aids in the superhydrophobic surface properties obtained for these films.

a)

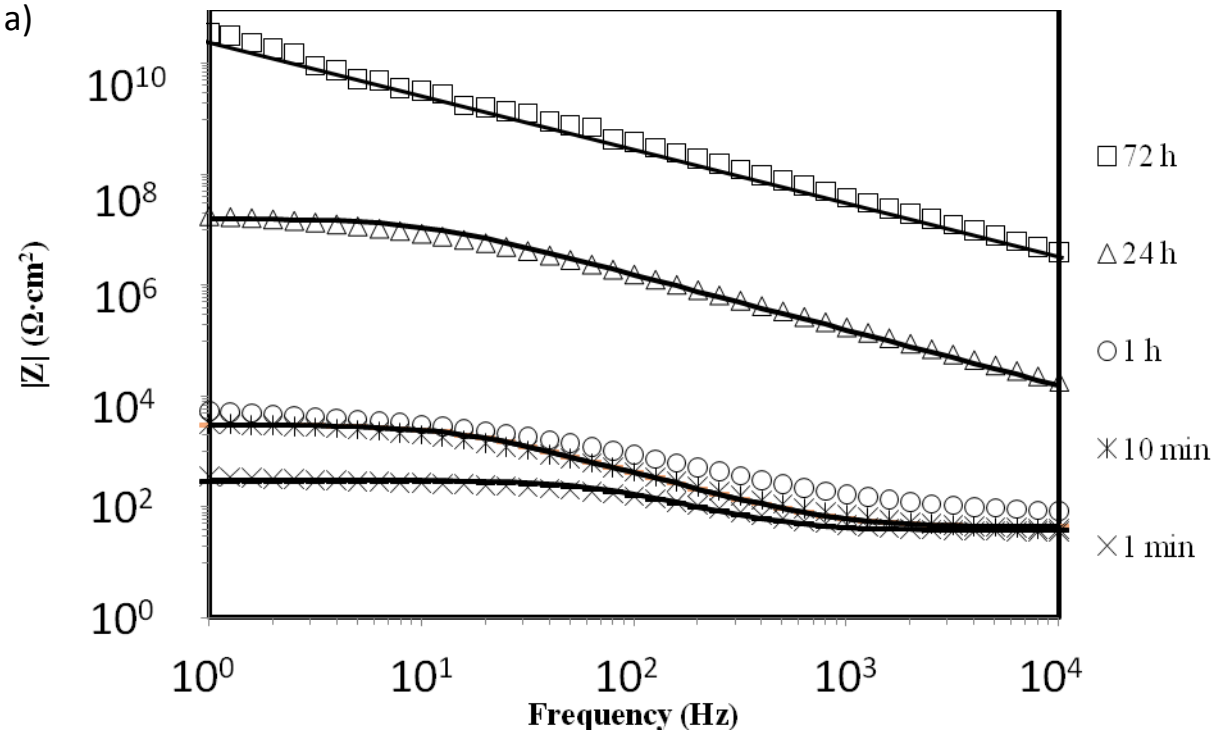
|Z| (Ω·cm²)
10¹⁰
10⁸
10⁶
10⁴
10²
10⁰
10⁰
10¹
10²
10³
10⁴
Frequency (Hz)
72 h
24 h
1 h
10 min
1 min

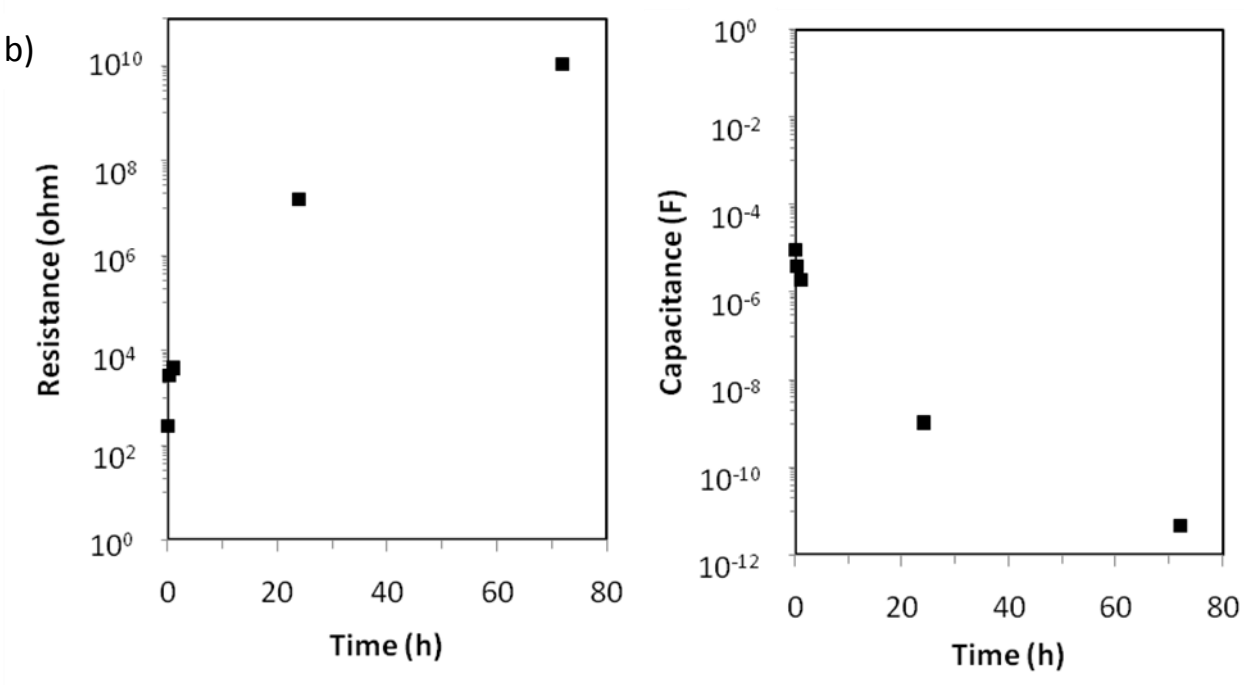

Figure 3.7. Electrochemical impedance spectra (a) and film resistance and capacitance data (b) obtained for PM films grown on borane-modified Au surfaces exposed to 8.5 mM DM in ether at -17 °C for the times indicated. The electrolyte solution consisted of $K_3Fe(CN)_6$ and $K_4Fe(CN)_6$ as redox probes in 0.1 M Na_2SO_4(aq).

Barrier Properties of PM Films

To analyze the time-dependence of barrier properties for PM films grown from borane-modified Au surfaces, I measured electrochemical impedance spectra of the films in 0.1M Na_2SO_4 solutions containing 1 mM $K_3Fe(CN)_6$ and 1mM $K_4Fe(CN)_6$ as redox probes. EIS enables measurement of the capacitance and resistance of the film after different periods of growth. Figure 3.7a shows impedance spectra in the form of Bode plots for PM films after various times of growth. A Bode plot will often show three distinctive regions in which solution resistance, film capacitance, or film resistance each govern the response. For the 1 min, 10 min, and 1 h exposures, small plateaus at high frequency depict the solution resistance, which is not visible in the spectra for longer exposures due to the larger impedance of the thicker polymer films. As frequency decreases, an incline in signal is shown in all spectra to indicate that film capacitance governs the response, so that the film functions as a dielectric that separates the conductive electrode from the electrolyte solution. The plateaus at low frequencies indicate the resistance by the film against the transport of the redox probes, with the value of the resistance scaling as the impedance modulus. As the polymerization is carried out over longer, there is an increase in film resistance coupled with a decrease in capacitance, thus indicating that with longer polymerization times and thicker films, the barrier properties are enhanced. A film resistance on the order of 10^{10}-10^{12} $\Omega \cdot cm^2$ and a capacitance of 4 x 10^{-12} F are achieved for a film that was allowed to polymerize for 72 h. Such huge resistances and small capacitances are unprecedented for polymer films grown from surfaces and/or general polymer films of this thickness. Figure 3.7 indicates a large increase in impedance from 24 to 72 h of polymerization time, yet there is only a modest

change in the IR plot for this same time window, which suggests that PM growth has slowed.

The inconsistency between the extent of film growth and the impedance suggests that the effective thickness or separation between the electrode and aqueous solution during EIS measurements is greater than the physical thickness of the PM films. Therefore, we theorize that an air film exists between the polymer and aqueous phase due the superhydrophobic nature of these films. Based on Cassie's equation for a drop of water on a superhydrophobic surface,

$$\cos\theta_c = X_{air}\cos\theta_{air} + X_{PM}\cos\theta_{PM}$$

$$X_{air} = 1 - X_{PM}$$

$$\cos 163^\circ = 1 - X_{PM}\cos 180^\circ + X_{PM}\cos 103^\circ$$

$$X_{PM} = 0.056$$

PM touches water at only ~6% of the surface. The remaining ~94% of PM/air interface would have a pronounced effect on impedance. Figure 3.8 illustrates what effect this air layer might be having. A film with a capacitance on the order of 10^{-12} F/cm^2 was exposed to 1,3,5-trichlorobenzene for 72 h. This solvent was chosen due to its ability to swell polymethylene and potentially destroy superhydrophobicity. After exposure to 1,3,5-trichlorobenzene, the impedance spectrum indicates an increase in capacitance by two orders of magnitude. The superhydrophobicity of this film was also destroyed in the process, perhaps negating the air effects theorized to affect initial capacitance. Figure 3.9

shows the IR spectrum of the PM film before and after exposure to TCB and reveals little change in the C-H bending signal to indicate that no appreciable amount of PM was lost during exposure. Therefore, the drop in capacitance upon exposure was not due to loss of PM itself but provides a rough estimate of the contribution by interfacial air layers and bubbles on the impedance response of a superhydrophobic polymer film. The wetting and impedance properties were not regained once the film was removed from the TCB.

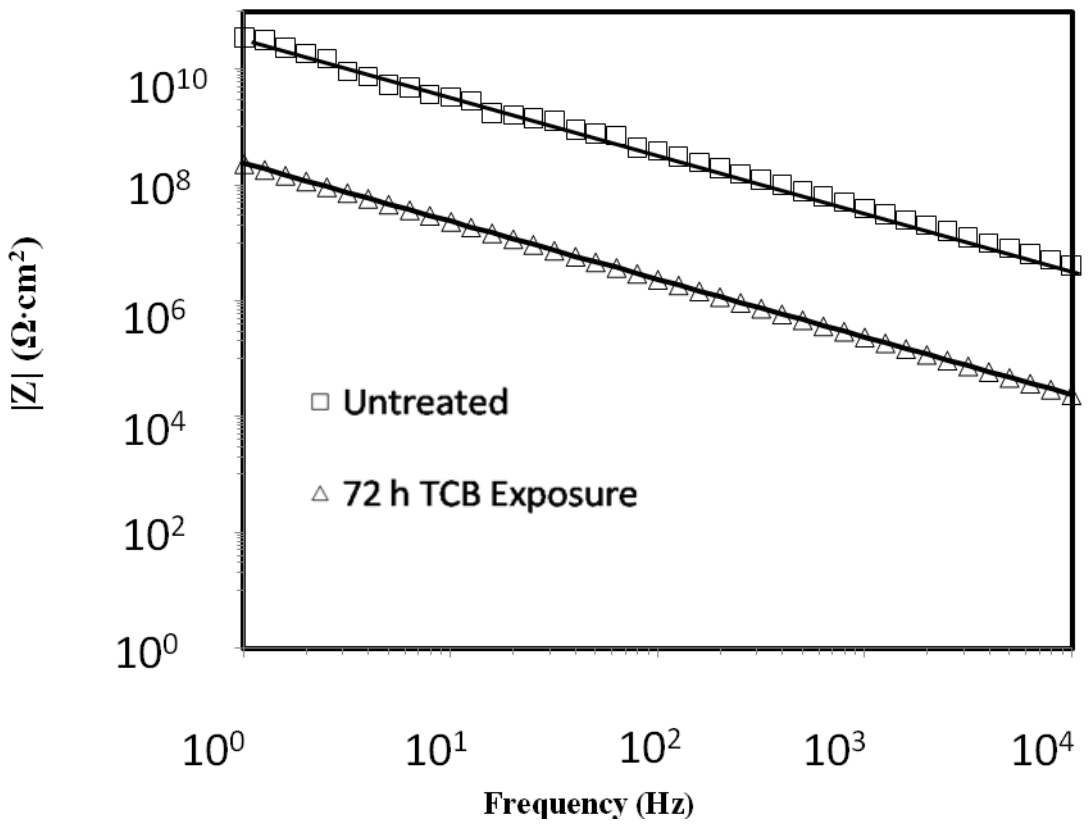

Figure 3.8. EIS spectra for a PM film grown from a hydroborated Au surface for 72 h before and after TCB exposure for 72 h.

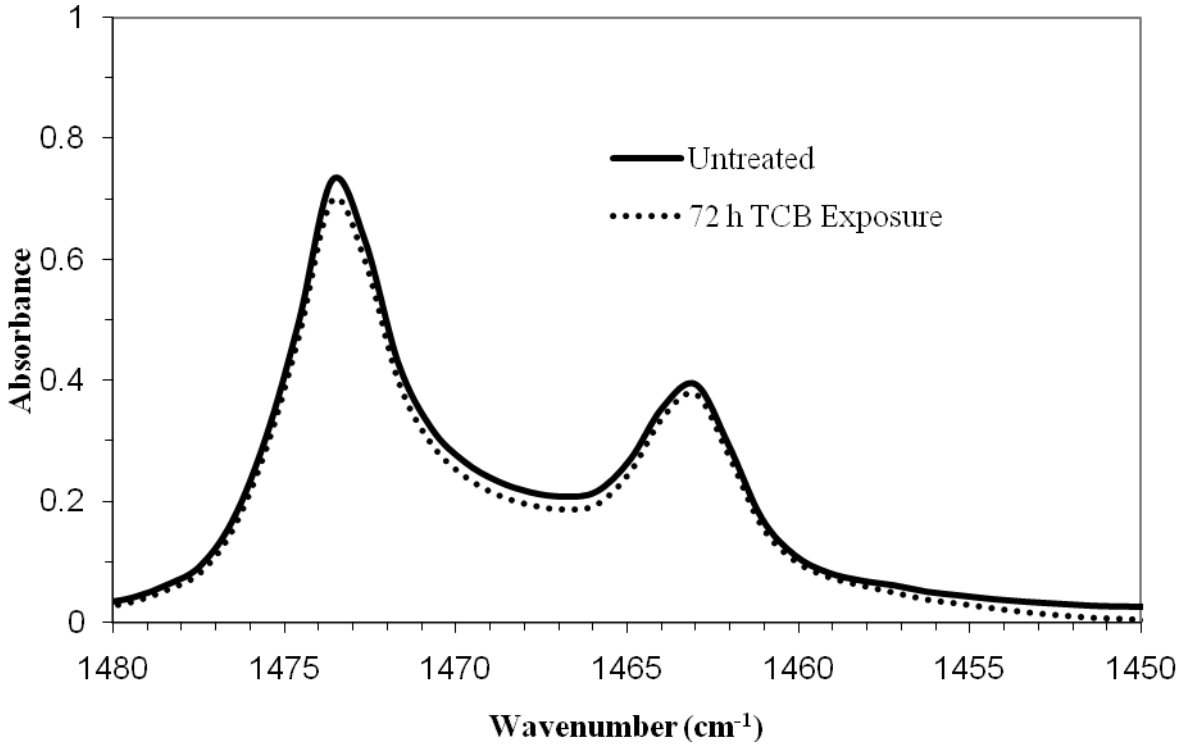

Figure 3.9. RAIR spectra of the C-H bending region for PM grown from hydroborated Au for 72 h before and after exposure to TCB for 72 h.

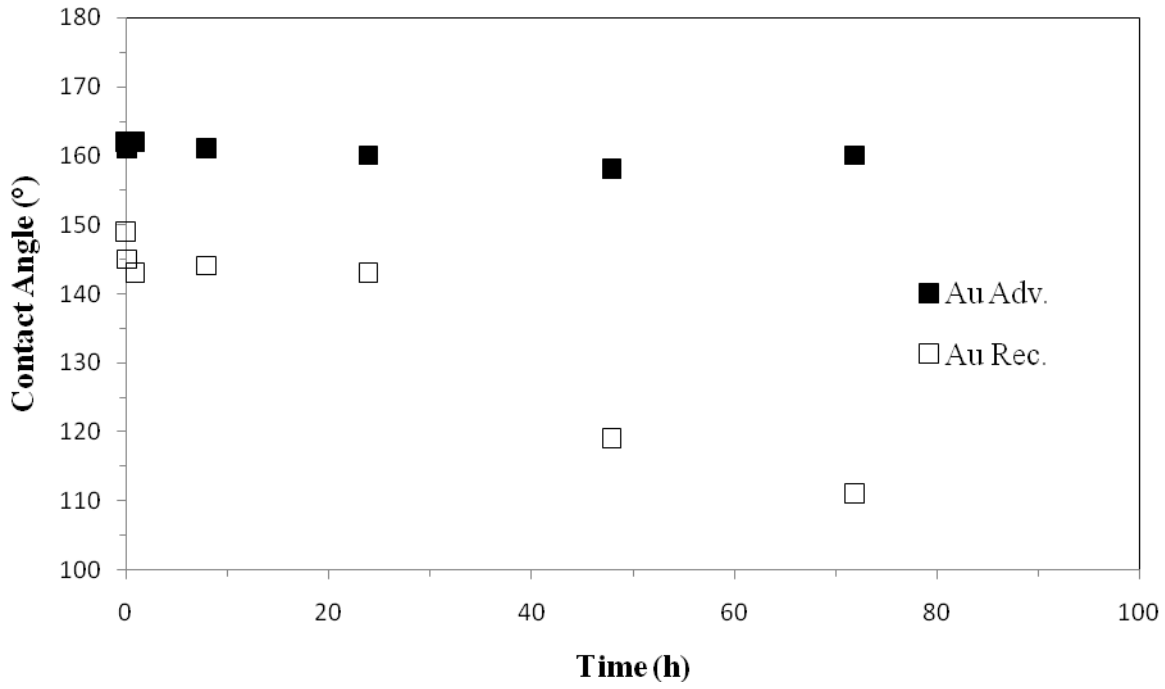

Figure 3.10. Effect of water exposure for times indicated on contact angles of PM films grown on borane-modified Au for 72 h by exposure to 8.5 mM DM in ether at -17°C.

Stability of the Superhydrophobic Property

The TCB study above indicates that exposure to solvents can alter the superhydrophobicity of the PM films. Therefore, I investigated other potential exposures that might affect film behavior as well. Figure 3.10 illustrates the stability of the superhydrophobic effect resist water penetration for PM films grown from borane-modified Au for 72 h. When the PM film is exposed to water constantly, the superhydrophobic nature of the film is lost as the receding contact angle falls from greater than 150° to approximately 140° after 1 h and to 110° after 72 h. However, the large advancing contact angle (>160°) only falls slightly throughout this exposure. This increase in hysteresis suggests that some type of structural change has taken place that

affects the surface wettability in a manner similar to the TCB exposure shown in Figure 3.10.

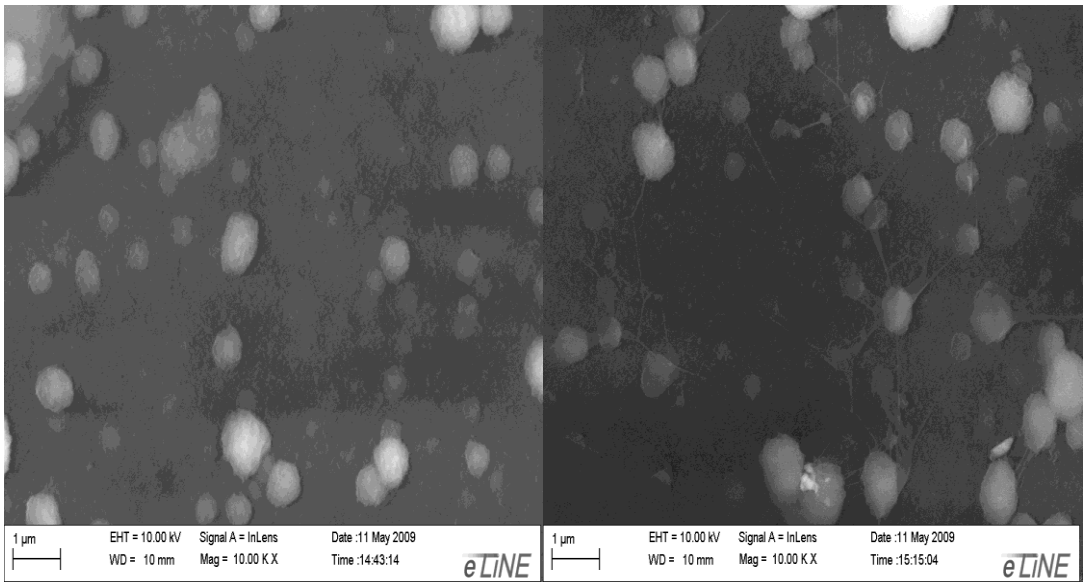

Figure 3.11. SEM image of a PM film on Au untreated (left) and after exposure to water (right) for 72 h.

Figure 3.11 illustrates the lack of change in the overall micro-scale structure of the PM film due to water exposure. Essentially no micron-scale topological changes are evident despite the loss of superhydrophobicity. Further investigation of the nanoscale structure before and after exposure via AFM might give further insight. One further note is that drying at low temperatures under vacuum was unable to recover the superhydrophobic nature of these films.

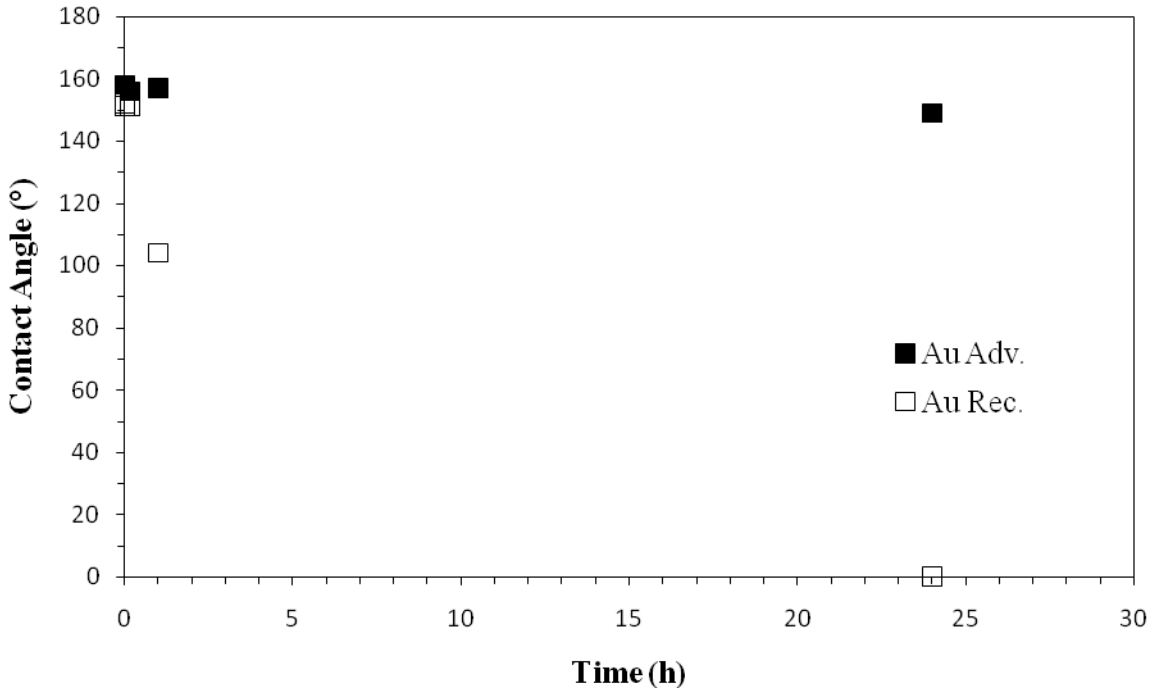

Figure 3.12. Effects of exposure to 135 °C temperature, in a vacuum oven, on contact angles of PM films grown on borane-modified Au for 72 h by exposure to 8.5 mM DM in ether at -17°C.

Similar to the wetting study shown above, we monitored contact angles for a PM film that was exposed to a temperature of 135°C for up to 24 h. This temperature was chosen as it approximates the melting temperature for polymethylene.[15] Examination of

Figure 3.12 reveals that the superhydrophobic nature of the film is affected in a little as 10 min. While the advancing angle remains high 155-160° throughout the duration of heat exposure, the receding angle drops dramatically, from an initial value of 150°, to nearly 100° in 1 h, and by the time the film has been exposed to this temperature for 24 h, the droplet no longer recedes. IR results show that there is no appreciable change in absorption signal yet there is an obvious change in the surface properties of this film. SEM images (Figure 3.13) suggest no significant micron-scale changes in film morphology. As mentioned above, the utilization of AFM images to examine the behavior of the nanoscale features with respect to this study could potentially give more insight into the loss of superhydrophobicity due to this heat exposure.

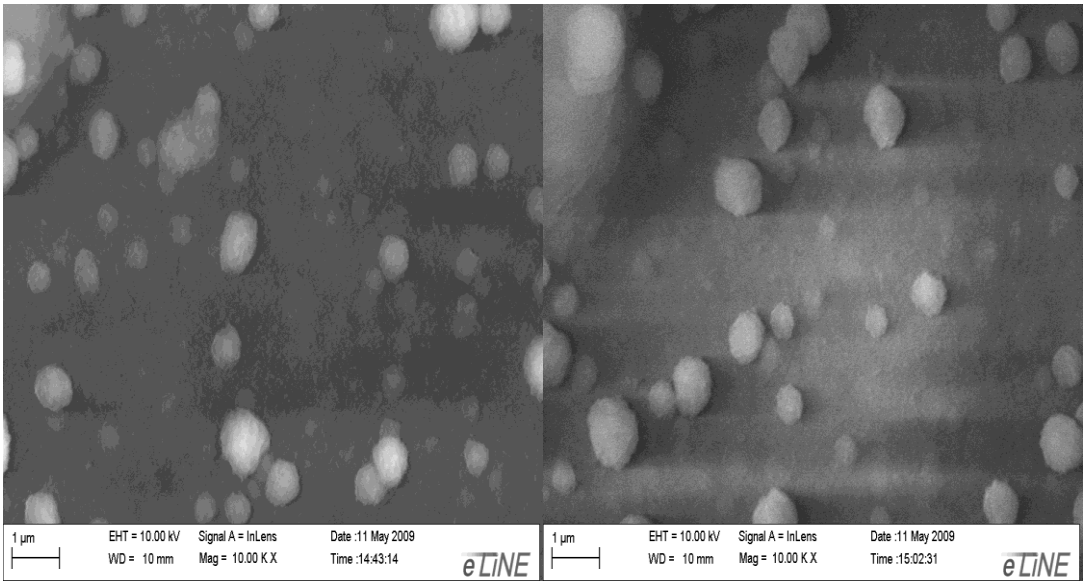

Figure 3.13. SEM image of a PM film untreated (left) and after exposure to reduced pressure at 135 °C (right) for 24 h.

Utilization of Heat Exposure

In addition to being able to demonstrate the stability of these PM films to water, heat, and solvent (TCB) exposures. I was able to utilize the degradation of superhydrophobicity at 135 °C temperature to demonstrate a potential application of these films. Using this knowledge, we applied localized heat exposure to a single site on a PM surface by touching the surface with a heated ball bearing whose temperature was ~150 °C. Then, upon allowing the surface to cool to room temperature, droplets of water were placed on the surface. Water contacting the untreated PM surface was quickly displaced from the flat surface; however, the droplets that contacted the heated region pooled at the site. The pool grew with increasing drops until it became too large to sustain itself and was then displaced and a new pool began to form. As such, these PM could potentially be patterned to direct water flow both to and away from certain areas on a scale as small as single drops.

Conclusions and Recommendations for Future Work

I have shown that surface-initiated polyhomologation enables the rapid preparation of superhydrophobic films, in as little as 10 min, with enhanced properties for prolonged polymerizations up to 72 h. Furthermore, the properties of the films grown from Au and Ag/Au surfaces were similar in thickness and morphology and likewise possessed similar surface and barrier properties. Other students in the Jennings group have demonstrated that these films can be grown from silicon surfaces. Therefore, we expect that these films can be grown from any surface that can be modified to contain borane groups via hydroboration.

With respect to the performance studies, I observed that long term (72 h) heat and water exposure irreversibly eliminated the superhydrophobic response. In addition, exposure to TCB produced the same result and minimal PM was lost, leading me to conclude that a surface morphological change was the cause of this loss of superhydrophobicity. SEM images revealed no apparent change in the micro-scale topology of the films due to these exposures. Further AFM imaging is needed to investigate the nanoscale morphology to better understand what structural changes may be occuring.

Lastly, the superhydrophobic properties on PM films grown from hydroborated Au and Ag/Au surfaces was destroyed with heat exposure at localized sites. This localized degradation of the wetting properties caused these localized sites to become "wells" for water accumulation while the remainder of the film still performed as a superhydrophobic barrier. Further investigation of this approach toward fine-tuned patterning could enable large surface areas of these films to be utilized for selective dewetting.

REFERENCES

1) Li, X.; Reinhoudt, D.; Crego-Calama, M.; "What do we need for a superhydrophobic surface? A review on the recent progress in the preparation of superhydrophobic surfaces;" *Royal Society of Chemistry* **2007**, 36, 1350-1368.

2) Sun, Y.; Qiao, R.; "Facile Tuning of Superhydrophobic States with Ag Nanoplates;" *Nano Research* **2008**, 1, 292-302.

3) Gao, L.; McCarthy, T.; "A Perfectly Hydrophobic Surface;" *J. Am. Chem. Soc.* **2006**, 128, 9052-9053.

4) Gao, L.; McCarthy, T.; "The "Lotus Effect" Explained: Two Reasons Why Two Length Scales of Topography Are Important;" *Langmuir* **2006**, 22, 2966-2967.

5) Gao, L.; McCarthy, T.; "Contact Angle Hysteresis Explained;" *Langmuir* **2006**, 22, 6234-6237.

6) Feng, X.; Jiang, L.; "Design and Creation of Superwetting/Antiwetting Surfaces;" *Adv. Mater.* **2006**, 18, 3063-3078.

7) Zhang, X.; Shi, F.; Niu, J.; Jiang, Y.; Wang, Z.; "Superhydrophobic surfaces; from structural control to functional application;" *J. Mater. Chem.* **2008**, 18, 621-633.

8) Ma, M.; Hill, R.; "Superhydrophobic surfaces;" *Current Opinion in Colloid & Interface Science II* **2006**, 193-202.

9) Love, J.C.; Estroff, L.A.; Kriebel, J.K.; Nuzzo, R.G.; Whitesides, G.M.; "Self-Assembled Monolayers of Thiolates on Metals as a Form of Nanotechnology;" *Chem. Rev.* **2005**, 105, 1103-1170.

10) Jennings, G.K.; Brantley, E.L.; "Physicochemical Properties of Surface-Initiated Polymer Films in the Modification and Processing of Materials;" *Adv. Mater.* **2004**, 16, 1983-1994.

11) Shah, R.R.; Merreceyes, D.; Husemann, M.; Rees, I; Abbott, N.L.; Hawker, C.J.; Hedrick, J.L.; "Using Atom Transfer Radical Polymerization To Amplify Monolayers of Initiators Patterned by Microcontact Printing into Polymer Brushes for Pattern Transfer;" *Macromolecules* **2000**, 33, 597-605.

12) Shea, K. J.; Walker, J. W.; Zhu, H.; Paz, M.; Greaves, J., Polyhomologation. A Living Polymethylene Synthesis. *J. Am. Chem. Soc.* **1997,** 119, 9049-9050.

13) Shea, K. J.; Staiger, C. L.; Lee, S. Y., Synthesis of Polymethylene Block Copolymers by the Polyhomologation of Organoboranes. *Macromolecules* **1999,** 32, 3157-3158.

14) Shea, K. J., Polyhomologation: The Living Polymerization of Ylides. *Chem. Eur. J.* **2000,** 6, 1113-1119.

15) Seshadri, K; Atre, S. V.; Tao, Y.-T.; Lee, M.-T.; Allara, D. L.; "Synthesis of Crystalline, Nanometer-Scale Polymethylene Clusters and Films on Gold Surfaces;" *J. Am. Chem. Soc.* **1997**, 119, 4698-4711.

16) Tao, Y.-T.; Pandian, K.; Lee, W.-C.; "Microfabrication of Interdigitated Polyaniline/Polymethylene Patterns on a Gold Surface;" *Langmuir* **1998**, 14, 6158-6166.

17) Guo, W.; Jennings, G.K.; "Use of Underpotentially Deposited Metals on Gold To Affect the Surface-Catalyzed Formation of Polymethylene Films;" *Langmuir* **2002**, 18, 3123-3126.

18) Guo, W.; Jennings, G.K.; "Directed Growth of Polymethylene Films on Atomically Modified Gold Surface;" *Adv. Mater.* **2003**, 15, 588-591.

19) Black, T.H.; "The Preparation and Reactions of Diazomethane;" *Aldrichimica Acta*, **1983**, 16, 3-10.

20) Bard, A.J; Faulkner, L.R.; *Electrochemical Methods: Fundamentals and Applications*; 2nd ed.; Wiley: New York, **2001**.

21) Bai, D.; Habersberger, B. M.; Jennings, G. K., pH-Responsive Copolymer Films by Surface-Catalyzed Growth. *J. Am. Chem. Soc.* **2005,** 127, 16486-16493.

22) Snyder, R.; "Vibrational correlation splitting and chain packing for the crystalline *n*-alkanes;" *J. Chem. Phys.* **1979**, 71(8), 3229-3235.

23) Quere, D.; "Wetting and Roughness;" *Annu. Rev. Mater. Res.* **2008**, 38, 71-90.

24) Zhu, L.; Xiu, Y.; Xu, J.; Tamirisa, P.A.; Hess, D.W.; Wong, C.-P.; "Superhydrophobicity on Two-Tier Rough Surfaces Fabricated by Controlled Growth of Aligned Carbon Nanotube Arrays Coated with Fluorocarbon;" *Langmuir*, **2005**, 21, 11208-11212.

25) McGuiness, C.L.; Shaporenko, A.; Mars, C.; Uppili, S.; Zharnikov, M.; Allara, D.L.; "Molecular Self-Assembly at Bare Semiconductor Surfaces: Preparation and Characterization of Highly Organized Octadecanethiolate Monolayers on GaAs(001);" *J. Am. Chem. Soc.* **2006**, 128, 5231-5243.